

Charge Order with Structural Distortion in Organic Conductors : Comparison between θ -(ET)₂RbZn(SCN)₄ and α -(ET)₂I₃

Yasuhiro TANAKA^{1*} and Kenji YONEMITSU^{1,2†}

¹*Institute for Molecular Science, Okazaki, Aichi 444-8585*

²*Graduate University for Advanced Studies, Okazaki, Aichi 444-8585*

Charge ordering with structural distortion in quasi-two-dimensional organic conductors θ -(ET)₂RbZn(SCN)₄ (ET=BEDT-TTF) and α -(ET)₂I₃ is investigated theoretically. By using the Hartree-Fock approximation for an extended Hubbard model which includes both on-site and intersite Coulomb interactions together with Peierls-type electron-lattice couplings, we examine the role of lattice degrees of freedom on charge order. It is found that the experimentally observed, horizontal charge order is stabilized by lattice distortion in both compounds. In particular, the lattice effect is crucial to the realization of the charge order in θ -(ET)₂RbZn(SCN)₄, while the peculiar band structure whose symmetry is lower than that of θ -(ET)₂RbZn(SCN)₄ in the metallic phase is also an important factor in α -(ET)₂I₃ together with the lattice distortion. For α -(ET)₂I₃, we obtain a phase transition from a charge-disproportionated metallic phase to the horizontal charge order with lattice modulations, which is consistent with the latest X-ray experimental result.

KEYWORDS: charge order, organic conductor, extended Hubbard model, electron-lattice coupling, Hartree-Fock approximation

1. Introduction

The family of quasi-two dimensional organic conductors (ET)₂X (ET=BEDT-TTF) exhibit a variety of interesting physical properties such as superconductivity, magnetism and charge order (CO).^{1,2} (ET)₂X consist of stacking layers of donor ET molecules and monovalent X anions. CO phenomena are observed in several members of (ET)₂X, which have a 3/4-filled π -electron band, and have been studied intensively since they have an important role to our understanding of electron correlation effects in low-dimensional systems.

θ -(ET)₂RbZn(SCN)₄^{3,4} and α -(ET)₂I₃^{5,6} are typical compounds that are known to exhibit CO. θ -(ET)₂RbZn(SCN)₄ shows a first-order metal-insulator transition at $T_c = 200$ K and a spin gap behavior at low temperatures much below T_c .⁷ The transition is accompanied by lattice distortion which changes its structure from the θ -type in the metallic phase to the so-called θ_d -type in the insulating phase. The CO formation below T_c has been directly observed by NMR experiments.^{3,4} Several experiments⁸⁻¹² such as Raman scattering¹⁰ and X-ray scattering^{11,12} measurements show that the horizontal-type CO is formed in this compound. In the metallic phase, X-ray experiments indicate a short-range CO with long periodicity, which is different from the horizontal-stripe state at low temperatures.^{11,12} The NMR measurement also shows slow fluctuations of CO in the metallic state.¹³ Similar charge fluctuations are observed in θ -(ET)₂CsZn(SCN)₄, which suggests the co-existence of charge modulations with different wave vectors^{14,15} although no long-range CO has been observed in this compound.

On the other hand, α -(ET)₂I₃ shows a metal-insulator

transition at $T = 135$ K,¹⁶ and a spin gap behavior is observed below T_c by the magnetic susceptibility measurement.¹⁷ Charge ordering in α -(ET)₂I₃ has been suggested theoretically by the Hartree-Fock approximation^{18,19} for the model that takes account of the full anisotropy of transfer integrals in this compound. Experimentally, the CO among ET molecules is confirmed by NMR experiments^{5,6} and Raman spectroscopy.²⁰ Moreover, it has been observed that the charge disproportionation exists even in the metallic state.^{20,21} The horizontal-type CO has been recently and directly observed by the X-ray scattering study,²² which also shows that the transition is accompanied by a structural distortion.²³⁻²⁵

Although the compounds θ -(ET)₂RbZn(SCN)₄ and α -(ET)₂I₃ have COs with very similar spatial patterns at low temperatures, the natures of the CO transitions are quite different. In θ -(ET)₂RbZn(SCN)₄, the transition is of first order and accompanied with a large lattice distortion and large discontinuity. On the other hand, the lattice distortion in α -(ET)₂I₃ is relatively small and, although the transition is of first order, the hysteresis of the specific heat is substantially smaller than that of θ -(ET)₂RbZn(SCN)₄.^{26,27} In fact, the recently observed photoinduced melting of CO in these compounds²⁸ shows a clear difference in the photoinduced dynamics, which is considered to originate from different roles of electron-lattice couplings in COs.

Theoretically, CO phenomena have been investigated by using the extended Hubbard model including on-site (U) and intersite (V_{ij}) Coulomb interactions.²⁹⁻⁴¹ The stability of various CO patterns in (ET)₂X has been discussed first within the Hartree approximation by considering the realistic band structures of (ET)₂X.^{2,29} The horizontal-stripe CO is shown to be stabilized in θ -

*yasuhiro@ims.ac.jp

†kxy@ims.ac.jp

(ET)₂RbZn(SCN)₄ and also in α -(ET)₂I₃. In particular, the horizontal CO is shown to be more stable in the θ_d -type structure than in the θ -type one, which suggests the lattice effects have an important role to realize the horizontal CO in θ -(ET)₂RbZn(SCN)₄. For θ -(ET)₂X, COs with long periodicity are also considered by several authors^{32,34–40} and they discussed their relevance to anomalous charge fluctuations in the metallic phase.

In the previous paper,⁴⁰ we have studied the effects of lattice distortion on CO in θ -(ET)₂X within the Hartree-Fock approximation by taking account of three Peierls-type electron-lattice couplings explicitly, which are deduced from the X-ray scattering experiment.⁴² The results show that the horizontal CO is stabilized by the lattice distortion, which results in the structural change from the θ -type to the θ_d -type. This is consistent with the experiments on θ -(ET)₂RbZn(SCN)₄ and also consistent with the recent numerical exact-diagonalization study.⁴¹

In this paper, we discuss the role of each electron-lattice coupling to the formation of CO in detail for θ -(ET)₂RbZn(SCN)₄. Furthermore, we consider the lattice effects in α -(ET)₂I₃ and compare the results with those for θ -(ET)₂RbZn(SCN)₄. It is found that although the lattice degrees of freedom are crucial to the realization of horizontal CO in θ -(ET)₂RbZn(SCN)₄, the effects are relatively small in α -(ET)₂I₃ where the band structure and Coulomb interactions have an important role. At finite temperatures, we compare the free energies of various CO patterns and investigate the CO phase transitions in both compounds. This paper is organized as follows. In §2, the extended Hubbard model and the Peierls-type electron-lattice couplings for θ -(ET)₂RbZn(SCN)₄ and α -(ET)₂I₃ are introduced. We show the results of the Hartree-Fock calculations at zero and finite temperatures and discuss their relevance to the experimental results in §3. §4 is devoted to the summary and conclusion.

2. Model and Method

2.1 Formulation

We consider the extended Hubbard model written as,

$$H = \sum_{\langle ij \rangle \sigma} (t_{i,j} + \alpha_{i,j} u_{i,j}) (c_{i\sigma}^\dagger c_{j\sigma} + \text{h.c.}) + U \sum_i n_{i\uparrow} n_{i\downarrow} + \sum_{\langle ij \rangle} V_{i,j} n_i n_j + \sum_{\langle ij \rangle} \frac{K_{i,j}}{2} u_{i,j}^2, \quad (1)$$

where $\langle ij \rangle$ represents the summation over the pairs of neighboring sites, $c_{i\sigma}^\dagger$ ($c_{i\sigma}$) denotes the creation (annihilation) operator for an electron with spin σ at the i th site, $n_{i\sigma} = c_{i\sigma}^\dagger c_{i\sigma}$, and $n_i = n_{i\uparrow} + n_{i\downarrow}$. The electron density is fixed at 3/4 filling. The electron-lattice coupling constant, lattice displacement and elastic constant are denoted by $\alpha_{i,j}$, $u_{i,j}$ and $K_{i,j}$, respectively. For the intersite Coulomb interactions $V_{i,j}$, we consider nearest neighbor interactions V_c for the vertical direction and V_p for the diagonal direction as shown in Fig. 1(a). We further rewrite the parameters for the lattice degrees of freedom by introducing new variables as $y_{i,j} = \alpha_{i,j} u_{i,j}$ and $s_{i,j} = \alpha_{i,j}^2 / K_{i,j}$. The actual form of $y_{i,j}$ together

with the transfer integrals $t_{i,j}$ for θ -(ET)₂RbZn(SCN)₄ and α -(ET)₂I₃ are given below. We apply the Hartree-Fock approximation

$$n_{i\sigma} n_{j\sigma'} \rightarrow \langle n_{i\sigma} \rangle n_{j\sigma'} + n_{i\sigma} \langle n_{j\sigma'} \rangle - \langle n_{i\sigma} \rangle \langle n_{j\sigma'} \rangle - \langle c_{i\sigma}^\dagger c_{j\sigma'} \rangle c_{j\sigma'}^\dagger c_{i\sigma} - c_{i\sigma}^\dagger c_{j\sigma'} \langle c_{j\sigma'}^\dagger c_{i\sigma} \rangle + \langle c_{i\sigma}^\dagger c_{j\sigma'} \rangle \langle c_{j\sigma'}^\dagger c_{i\sigma} \rangle \quad (2)$$

to eq. (1) and the obtained Hamiltonian is diagonalized in k -space by assuming unit cells of various mean-field order parameters. We consider four types of order parameters according to the alignment of hole-rich molecules, namely, 3-fold, diagonal, horizontal and vertical COs which are schematically shown in Fig. 2. As for the spin degrees of freedom, we use three spin configurations in each stripe-type CO which are identical to those of ref. 29, while the antiferromagnetic state between hole-rich and -poor sites is considered in the 3-fold CO. The ground-state energy is calculated by solving the mean-field equation self-consistently together with the lattice displacements, which are determined by the Hellmann-Feynman theorem. The energy per site is given by

$$E = \frac{1}{N} \left(\sum_{l\mathbf{k}\sigma} E_{l\mathbf{k}\sigma} n_F(E_{l\mathbf{k}\sigma}) - U \sum_i \langle n_{i\uparrow} \rangle \langle n_{i\downarrow} \rangle - \sum_{\langle ij \rangle} V_{ij} \langle n_i \rangle \langle n_j \rangle + \sum_{\langle ij \rangle \sigma} V_{ij} \langle c_{i\sigma}^\dagger c_{j\sigma} \rangle \langle c_{j\sigma}^\dagger c_{i\sigma} \rangle + \sum_{\langle ij \rangle} \frac{y_{ij}^2}{2s_{ij}} \right), \quad (3)$$

where l , $E_{l\mathbf{k}\sigma}$ and n_F is a band index, an energy eigenvalue of the mean-field Hamiltonian and the Fermi distribution function, respectively. N is the total number of sites. We notice that the presence or absence of the Fock terms in eq. (2) does not alter the qualitative results including the lattice displacements although the energy of each self-consistent solution is lowered by the Fock terms.

At finite temperatures we calculate the free energy within the Hartree-Fock approximation. The free energy per site is written as

$$F = \frac{1}{N} \left(\mu N_{tot} - \frac{1}{\beta} \sum_{l\mathbf{k}\sigma} \ln(1 + \exp\{-\beta(E_{l\mathbf{k}\sigma} - \mu)\}) - U \sum_i \langle n_{i\uparrow} \rangle \langle n_{i\downarrow} \rangle - \sum_{\langle ij \rangle} V_{ij} \langle n_i \rangle \langle n_j \rangle + \sum_{\langle ij \rangle \sigma} V_{ij} \langle c_{i\sigma}^\dagger c_{j\sigma} \rangle \langle c_{j\sigma}^\dagger c_{i\sigma} \rangle + \sum_{\langle ij \rangle} \frac{y_{ij}^2}{2s_{ij}} \right), \quad (4)$$

where μ , N_{tot} and β is the chemical potential, total number of electrons and inverse of temperature, respectively.

2.2 θ -(ET)₂RbZn(SCN)₄

The structure of θ -(ET)₂RbZn(SCN)₄ in the metallic phase and that in the CO phase are shown in Figs. 1(a) and 1(b), respectively. In the metallic phase, there are two kinds of transfer integrals t_p and t_c for diagonal and vertical bonds, while the CO transition doubles the

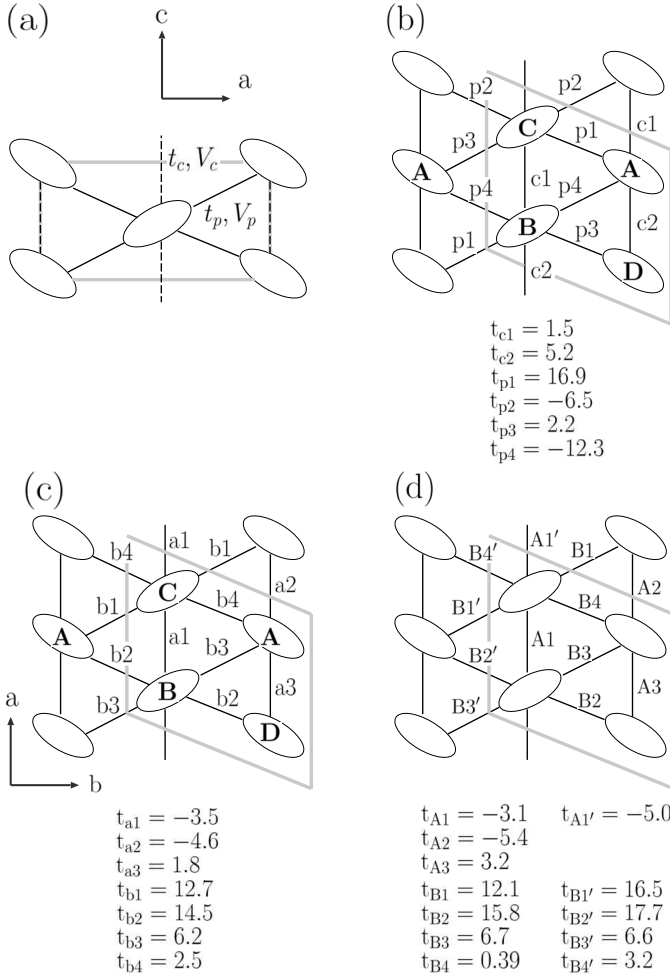


Fig. 1. Schematic representations of the structures of (a) θ -(ET) $_2$ X, (b) θ -(ET) $_2$ RbZn(SCN) $_4$ in the CO phase, (c) α -(ET) $_2$ I $_3$ in the metallic phase, and (d) α -(ET) $_2$ I $_3$ in the CO phase. The gray solid lines indicate the unit cell. For (b), (c), and (d), the transfer integrals estimated by the extended Hückel method^{11, 22} are also shown. For α -(ET) $_2$ I $_3$, the site indices A, B, C, and D in our notation correspond to A, B, C, and A', respectively, in the conventional notation.⁴³

unit cell in the c -direction and six transfer integrals exist at low temperatures. In order to take account of the lattice effects, we consider three kinds of electron-lattice couplings, $s_{i,j}$: s_c , s_a , and s_ϕ that originate from the c - and a -axis molecular translations and molecular rotation, respectively. They have been introduced in the previous papers,^{40, 41} being suggested by the X-ray experiment that shows rather complicated displacements of ET molecules through the CO transition.¹¹ First, the c -axis translation alternates t_c . This modulation gives t_{c1} and t_{c2} in Fig. 1(b). Similarly, the a -axis translation induces the modulation of t_{p1} and t_{p3} . Finally, the rotational degrees of freedom are taken into account by the changes in t_{p2} and t_{p4} . This type of modulation is expected to be important since the horizontal CO is formed on the t_{p4} chains with hole-rich molecules. In fact, the experimental estimation¹¹ indicates that the dependence of transfer integrals on a relative angle (called elevation angle¹¹) of neighboring ET molecules is large and allows uniformly decreasing (increasing) $|t_{p2}|$ ($|t_{p4}|$) on the horizontally

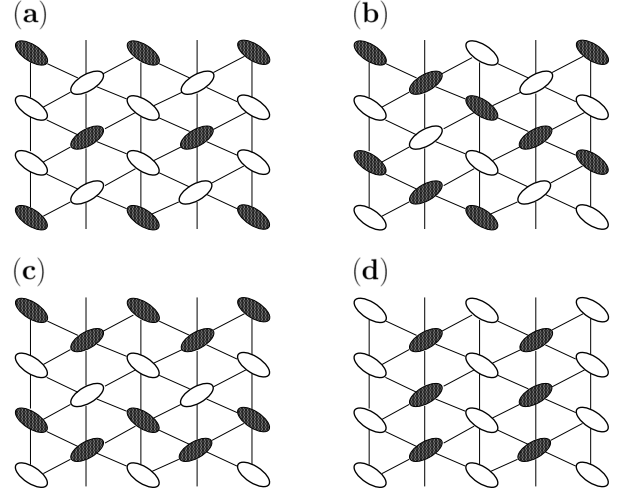


Fig. 2. Spatial patterns of COs considered in the Hartree-Fock calculations. (a)3-fold, (b)diagonal-stripe, (c)horizontal-stripe, and (d)vertical-stripe COs. The hole-rich and hole-poor sites are denoted by the solid and open ellipses, respectively.

connected bonds. These three kinds of electron-lattice couplings cause the modulations $y_{i,j}$ of transfer integrals that are experimentally observed. For simplicity, they are assumed to be independent and we do not consider any other electron-lattice coupling. Then, the transfer integrals in the distorted structure are given by,

$$\begin{aligned}
 t_{c1} &= t_c + y_c, \\
 t_{c2} &= t_c - y_c, \\
 t_{p1} &= t_p + y_a, \\
 t_{p2} &= t_p - y_\phi, \\
 t_{p3} &= t_p - y_a, \\
 t_{p4} &= t_p + y_\phi,
 \end{aligned} \tag{5}$$

where y_c , y_a , and y_ϕ are modulations due to s_c , s_a , and s_ϕ , respectively. Here the signs in eq. (5) are chosen so that the transfer integrals realized experimentally at low temperatures correspond to $y_l > 0$ for $l = c, a$ and ϕ .⁴⁰ In the calculations, we use $t_p = 0.1(\text{eV})$ and $t_c = -0.04$ in the high temperature phase for $t_{i,j}$ in eq. (1). Then, the modulations y_c , y_a , and y_ϕ are self-consistently determined for each set of electron-lattice coupling constants.

2.3 α -(ET) $_2$ I $_3$

The transfer integrals for α -(ET) $_2$ I $_3$ in the high- and low-temperature phases are shown in Figs. 1(c) and 1(d), respectively. The unit cell contains four molecules in both phases. According to the X-ray structural analysis,²² sites A and D are equivalent to each other owing to the inversion symmetry in the metallic phase, while the symmetry breaks below the CO transition temperature. Sites A and B (C and D) become hole-rich (hole-poor) in the horizontal CO state. The large transfer integrals, t_{b1} and t_{b2} , form a one-dimensional zigzag chain in the conducting layer. The extended Hückel calculation indicates that they gradually increase with decreasing temperature.²² At the CO transition, t_{b1} changes into t_{B1} and

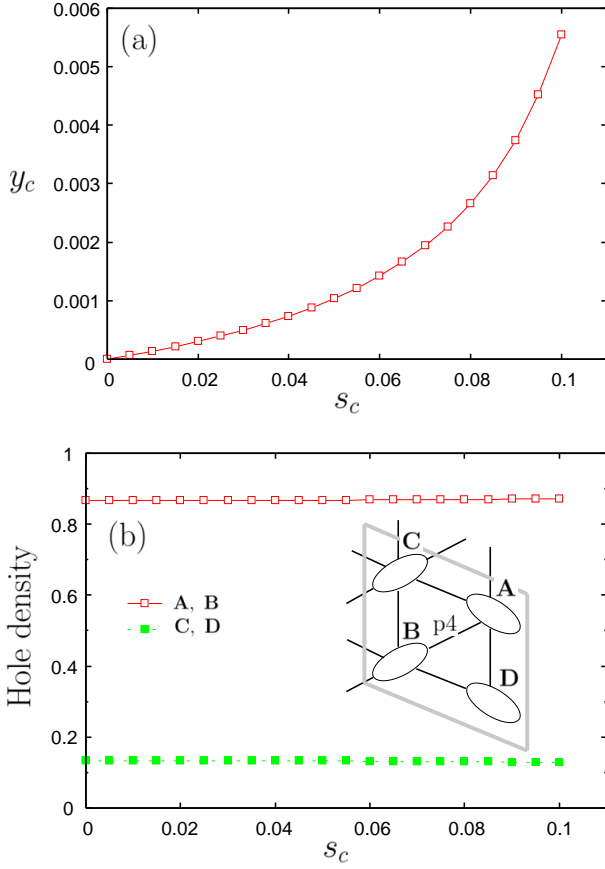


Fig. 3. (Color online) (a) Modulation y_c and (b) hole densities as a function of s_c for $U = 0.7$, $V_c/U = 0.35$, and $V_p/V_c = 0.7$.

$t_{B1'}$ in Fig. 1(d), while t_{b2} becomes t_{B2} and $t_{B2'}$. The other transfer integrals with smaller values also change at the transition. The lattice modulation in this system is suggested to come mainly from the molecular rotation rather than the translational shifts of the molecules.²²

In the present paper, we investigate the lattice effects on the system by taking account of the modulations in t_{b1} and t_{b2} . We do not consider the modulations in smaller transfer integrals than the above ones. These effects will be mentioned in the following section. As in the case of θ -(ET)₂RbZn(SCN)₄, we let s_{b1} and s_{b2} denote the electron-lattice couplings that change t_{b1} and t_{b2} , respectively. The corresponding modulations are written as y_{b1} and y_{b2} . The transfer integrals in the low temperature phase are then written as

$$\begin{aligned} t_{B1'} &= t_{b1} + y_{b1} , \\ t_{B1} &= t_{b1} - y_{b1} , \\ t_{B2'} &= t_{b2} + y_{b2} , \\ t_{B2} &= t_{b2} - y_{b2} , \end{aligned} \quad (6)$$

where the signs in eq. (6) are again chosen so as for positive values to correspond to the modulations realized in α -(ET)₂I₃. The other transfer integrals are assumed to be unchanged. For the values of $t_{i,j}$ in eq. (1) with which the Hartree-Fock calculations are carried out, we use those in the high temperature phase that are shown

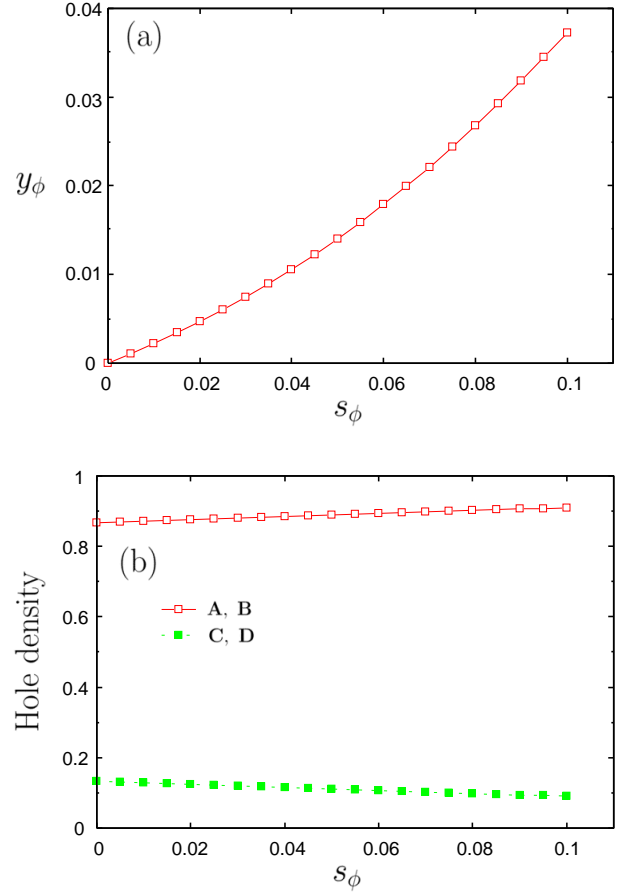


Fig. 4. (Color online) (a) Modulation y_ϕ and (b) hole densities as a function of s_ϕ for $U = 0.7$, $V_c/U = 0.35$, and $V_p/V_c = 0.7$.

in Fig. 1(c).

3. Results and Discussions

3.1 θ -(ET)₂RbZn(SCN)₄

First, let us consider the effect of each electron-lattice coupling on the horizontal CO that is experimentally observed in θ -(ET)₂RbZn(SCN)₄. Figures 3, 4 and 5 show the lattice displacements and order parameters as a function of the electron-lattice coupling when we assume the horizontal CO as the mean-field order parameter for $U = 0.7$, $V_c/U = 0.35$, and $V_p/V_c = 0.7$. Note that the obtained CO state is not the ground state for small electron-lattice couplings, as we will discuss later. From Figs. 3(a) and 4(a), we can see that y_c and y_ϕ increase with increasing s_c and s_ϕ , respectively. The modulations grow linearly for small s_c and s_ϕ , which indicates that the horizontal CO is stabilized by these lattice modulations. The hole density at each site in the unit cell shows that the disproportionation is enlarged by s_ϕ although the dependence is weak in the case of s_c . On the other hand, the behavior of y_a is different from the above two modulations, as shown in Fig. 5. y_a becomes nonzero when s_a exceeds some value. With the increase of y_a , the order parameter tends to decrease, which shows the y_a modulation suppresses the charge disproportionation in the horizontal CO. The energy gain by these electron-lattice couplings is shown in Fig. 6. We find that the effect of s_ϕ

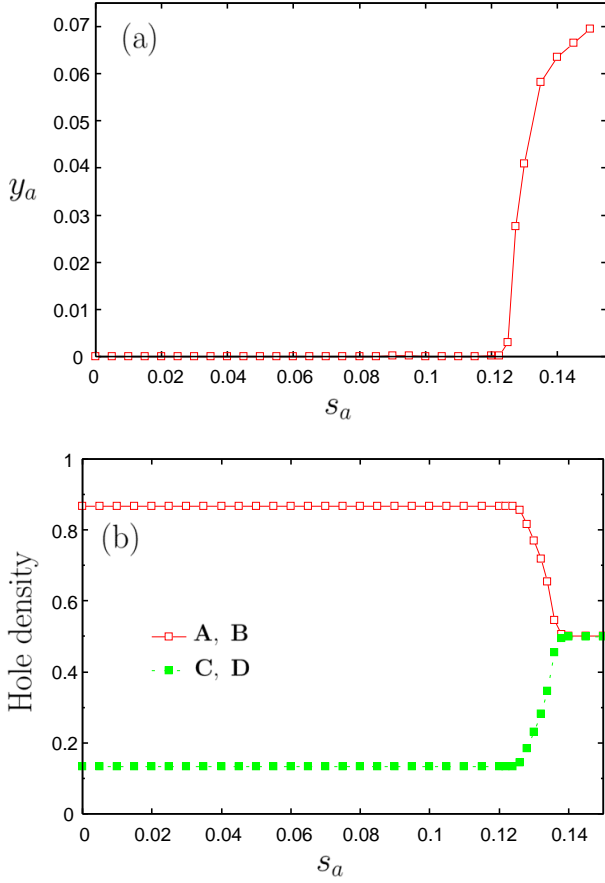


Fig. 5. (Color online) (a) Modulation y_a and (b) hole densities as a function of s_a for $U = 0.7$, $V_c/U = 0.35$, and $V_p/V_c = 0.7$.

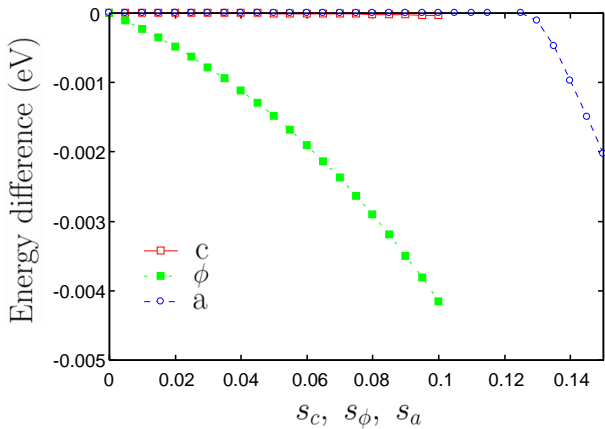


Fig. 6. (Color online) Energy gain due to each electron-lattice coupling in the horizontal CO for $U = 0.7$, $V_c/U = 0.35$, and $V_p/V_c = 0.7$.

is the largest. Since the horizontal stripe CO is formed on the hole-rich sites that are connected by the t_{p4} chain, the y_ϕ modulation lowers the energy through the exchange coupling between neighboring spins on the stripe. The energy gain due to spin fluctuations is also obtained by the perturbation theory from the strong-coupling limit, i.e., $t_{i,j} = 0$.⁴¹

Next, we discuss the stability of various CO patterns.

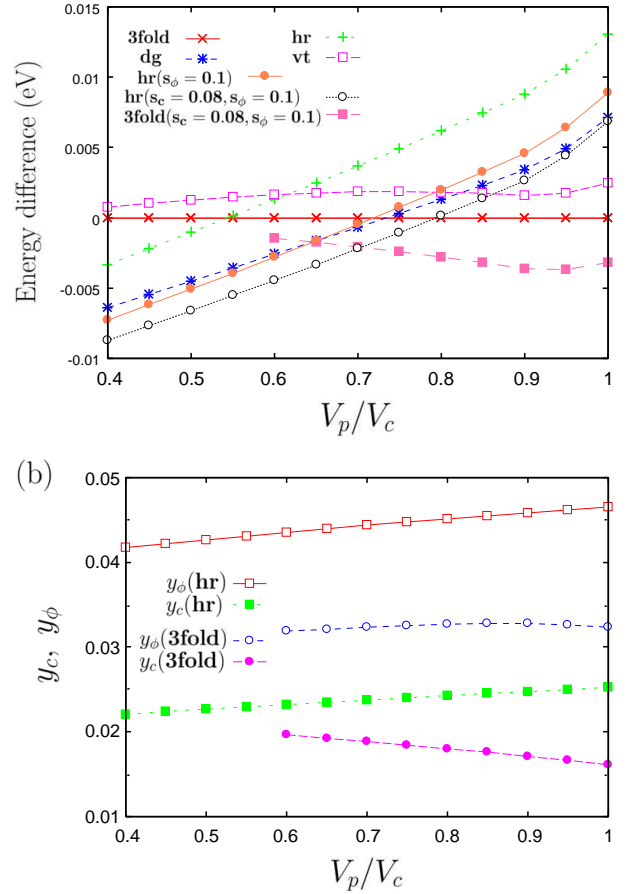


Fig. 7. (Color online) (a) Ground-state energies for various CO states as a function of the ratio V_p/V_c for $U = 0.7$ and $V_c/U = 0.35$. The energy of 3-fold CO is chosen to be zero. hr, dg, and vt mean the horizontal, diagonal, and vertical COs, respectively. (b) Modulations in the transfer integrals for the horizontal and 3-fold COs.

The ground-state energies as a function of V_p/V_c are compared in Fig. 7(a). In this figure, the energy of the 3-fold CO without electron-lattice couplings is set at zero. We have shown only the lowest energy state for each CO pattern among different spin configurations. In the absence of electron-lattice couplings, the 3-fold CO with a ferromagnetic spin configuration is the most favorable in the nearly isotropic region, $V_p/V_c \sim 1$, while the diagonal CO whose spin configuration is antiferromagnetic along the stripe and between stripes on the c -axis is stable when V_p/V_c is small, $V_p/V_c < 0.7$.^{34,40} For the horizontal CO, we plotted the energy of the state that is antiferromagnetic along the stripe and ferromagnetic between stripes on the c -axis. The state that is antiferromagnetic on the c -axis has a close energy and is nearly degenerate with the above state. Without electron-lattice coupling, the energy of the horizontal CO cannot be the lowest in any region.

Figure 7(a) shows that the electron-lattice couplings stabilize the horizontal CO considerably. Here, we concentrate on the effects of s_c and s_ϕ separately since the results in the case where the three electron-lattice couplings are simultaneously present have been shown previously.⁴⁰ The diagonal and vertical COs are not affected

by s_c and s_ϕ , then the horizontal CO becomes more stable than these states. The values of the electron-lattice couplings are chosen to be $s_c = 0.08$ and $s_\phi = 0.1$. The resultant lattice displacements are shown in Fig. 7(b), which are comparable to the experimentally observed values. The horizontal CO has hole-rich sites on the t_{p4} chains, which is consistent with the experimental findings. The 3-fold CO also has energy gain from the lattice modulations due to s_c and s_ϕ . To obtain the mean-field solution for the 3-fold CO that coexists with lattice modulations, we have assumed the unit cell of 2×6 sites in the a - c plane. In this state, a weak horizontal charge modulation is caused by the lattice distortion in the background of the 3-fold CO. The distortions in transfer integrals are weak compared to those in the horizontal CO. Note that the 3-fold CO is metallic even if the transfer integrals are modulated while the horizontal CO is insulating. In short, the horizontal CO with lattice distortion becomes stable for $V_p/V_c < 0.7$, while the 3-fold CO is favorable for $0.7 < V_p/V_c \lesssim 1$.

Here we briefly mention the effect of s_a . Since the y_a distortion reduces the horizontal CO, y_c and y_ϕ tend to be suppressed when y_a is large.⁴⁰ The energy of the horizontal CO is only slightly lowered by this y_a distortion. The relative stability of this CO compared to the others in the range of $V_p/V_c < 0.7$ is unchanged as long as we choose s_a to obtain the experimentally observed value of y_a .

At finite temperatures, the stability of COs is investigated by calculating the free energy within the Hartree-Fock approximation. The used values of U , V_c/U , and the electron-lattice couplings are the same as those for $T = 0$. The temperature dependences of the free energies for various CO patterns are shown in Figs. 8(a) and 8(b) in the cases of $V_p/V_c = 1.0$ and $V_p/V_c = 0.69$, respectively. For $V_p/V_c = 1.0$, the 3-fold CO is the most stable state in a wide temperature range. On the other hand, the horizontal CO with lattice modulations becomes more stable when V_p/V_c is small. In particular, a first-order metal-insulator transition between the 3-fold CO and the horizontal CO occurs for smaller values of V_p/V_c than unity, as shown in Fig. 8(b) where the transition is located at $T_c \sim 0.025$.

The first-order metal-insulator transition at a finite temperature can be related to the experimental results of θ -(ET)₂RbZn(SCN)₄ although the wave vector of the charge modulation in the 3-fold CO state is different from that of the experiments in the metallic phase. It has recently been proposed that the experimental observation can be reproduced by considering Coulomb interactions extended to a longer range than the nearest-neighbor sites.³⁶ As for the spin degrees of freedom, both the 3-fold and the horizontal COs in our Hartree-Fock calculation have spin orders which have not been observed in the experiments. The effect of quantum fluctuations is necessary in discussing the behavior of the spin degrees of freedom.

The estimation of the intersite Coulomb interactions V_p and V_c indicates that these values are comparable,⁴⁴ $V_p/V_c \sim 1$, where the 3-fold CO is the most stable in our calculation. A variational Monte Carlo study³⁵ for

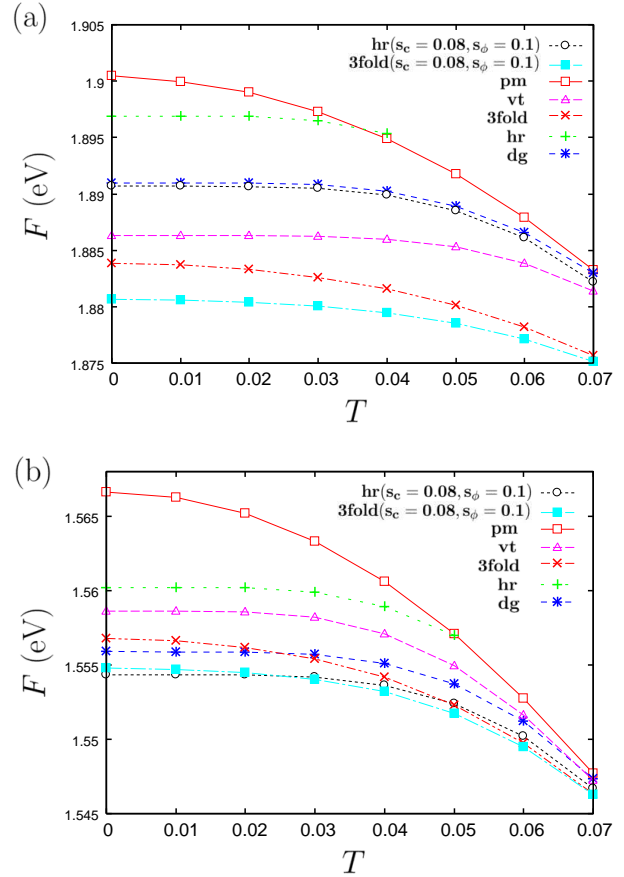


Fig. 8. (Color online) Free energies for various CO patterns for (a) $V_p/V_c = 1.0$ and (b) $V_p/V_c = 0.69$ in the case of $U = 0.7$ and $V_c/U = 0.35$. pm means the paramagnetic metallic state with uniform charge density. A first-order metal-insulator transition from the 3-fold CO to the horizontal CO occurs at $T_c \sim 0.025$.

the extended Hubbard model without electron-lattice couplings also shows that the 3-fold CO is stable for $V_p/V_c \sim 1$. According to the recent exact-diagonalization study,⁴¹ the horizontal CO with lattice distortions becomes more stable even at $V_p/V_c \sim 1$ if we take account of quantum fluctuations that are neglected in the Hartree-Fock approximation. It is also indicated that the Holstein-type electron-lattice coupling stabilizes the horizontal CO by an exact-diagonalization study.³¹

We find that the 3-fold state with coexisting weak horizontal charge modulation is stable at the nearly isotropic region $V_p/V_c \sim 1$. This can be related to the X-ray diffraction results on θ -(ET)₂CsZn(SCN)₄,^{14,15} which show two types of COs coexisting as short-range fluctuations. Although the present Hartree-Fock calculation gives an artificial long-range CO, quantum fluctuations are expected to destroy the long-range order and result in a state where different types of COs coexist as short-range fluctuations.

3.2 α -(ET)₂I₃

As in the previous subsection, we first discuss the effects of two electron-lattice couplings s_{b1} and s_{b2} on the horizontal CO. In the CO state, sites A and B are hole-rich, while sites C and D are hole-poor. The spin configuration is antiferromagnetic along the stripe and

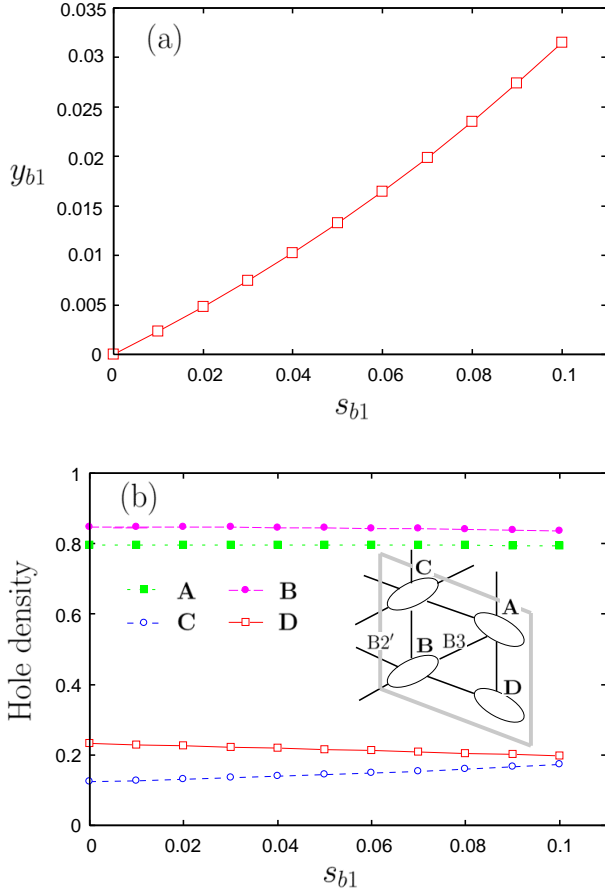


Fig. 9. (Color online) (a) Modulation y_{b1} and (b) hole densities as a function of s_{b1} for $U = 0.7$, $V_c/U = 0.4$ and $V_p/V_c = 0.8$.

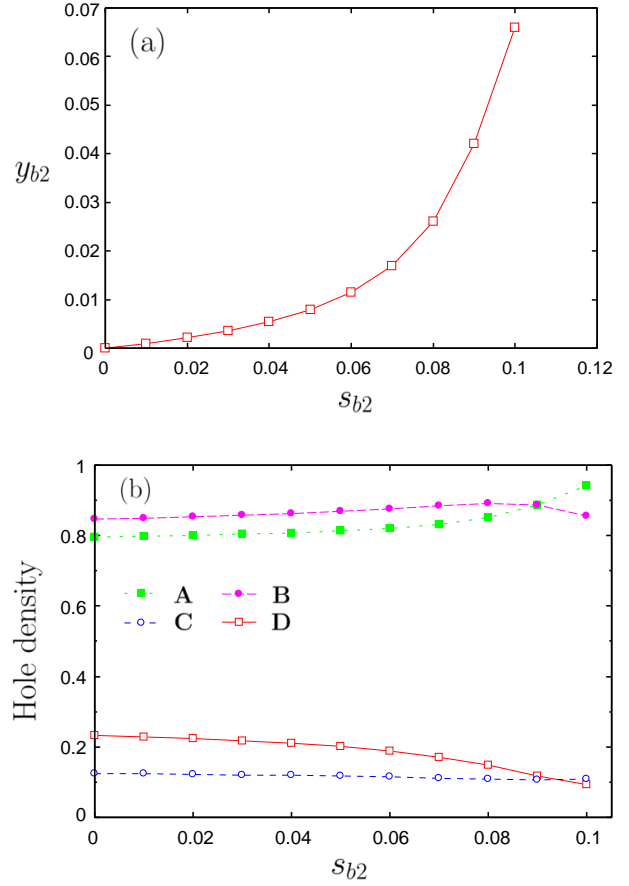


Fig. 10. (Color online) (a) Modulation y_{b2} and (b) hole densities as a function of s_{b2} for $U = 0.7$, $V_c/U = 0.4$ and $V_p/V_c = 0.8$.

ferromagnetic between the stripes. We choose $U = 0.7$, $V_c/U = 0.4$, and $V_p/V_c = 0.8$ here. Figures. 9 and 10 show the lattice displacements and order parameters for the horizontal CO in the presence of s_{b1} and s_{b2} , respectively. Although the charge distribution does not change largely, the displacements increase with increasing the electron-lattice coupling in both cases, which shows that these couplings stabilize the horizontal CO. This can be seen from the energy gain due to the distortions. As shown in Fig. 11, the energy of the horizontal CO is lowered in the presence of s_{b1} and s_{b2} .

The ground-state energies of various CO patterns per site are compared in Fig. 12(a). We set $U = 0.7$, $V_c/U = 0.4$ here. The electron-lattice couplings are chosen to be $s_{b1} = 0.08$ and $s_{b2} = 0.05$. The 3-fold CO has a ferromagnetic spin configuration in the 2×6 unit cell as in the case of the θ -type salt. For the vertical CO, the energies of two solutions that are nearly degenerate are shown. vt1 means the vertical CO with hole-rich sites A and D whereas vt2 denotes the one with hole-rich sites B and C. For vt1, the spins on the stripes are antiferromagnetic and those between the stripes are ferromagnetic. vt2 has a ferromagnetic spin configuration on the stripes and an antiferromagnetic one between the stripes. It can be seen from Fig. 12(a) that the 3-fold CO is the most stable near the isotropic repulsions, i.e., $V_p/V_c \sim 1$. When the anisotropy in V_p/V_c is large, i.e., $V_p/V_c < 0.65$,

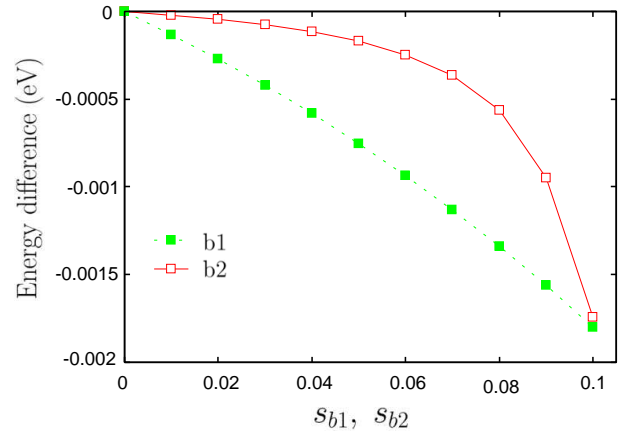


Fig. 11. (Color online) Energy gain due to each electron-lattice coupling in the horizontal CO for $U = 0.7$, $V_c/U = 0.4$, and $V_p/V_c = 0.8$.

on the other hand, the horizontal CO is more stable than the other CO states even in the absence of electron-lattice couplings. This has been pointed out within the Hartree approximation.²⁹ This is in contrast to the θ -type salt where the horizontal CO does not become the ground state without electron-lattice couplings. Therefore, the band structure which originates from the vari-

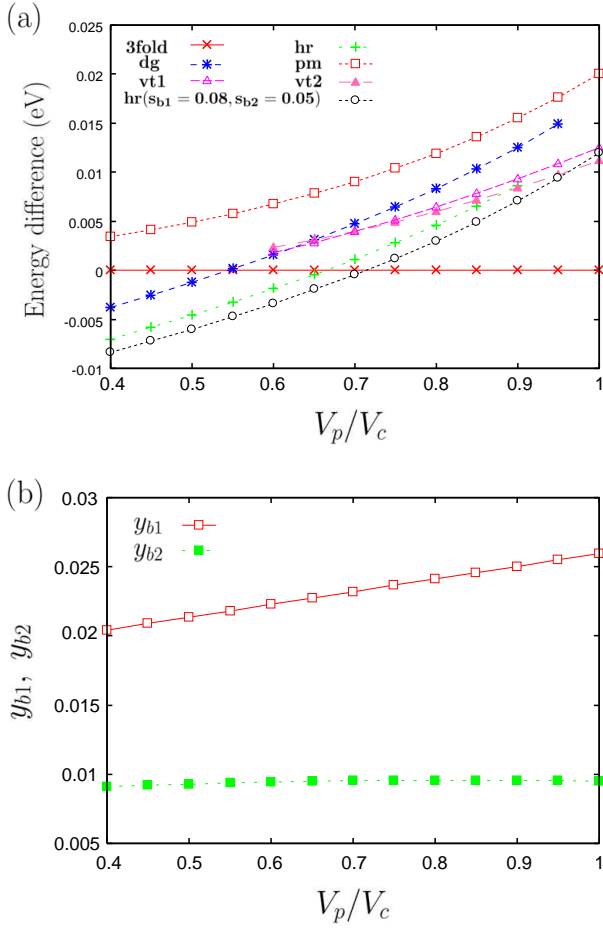


Fig. 12. (Color online) (a) Ground-state energies for various CO states as a function of the ratio V_p/V_c for $U = 0.7$ and $V_c/U = 0.4$. (b) Modulations in the transfer integrals for the horizontal CO.

ety of transfer integrals in the high temperature phase is considered to have an important role to stabilize the CO in the α -type salt. In the presence of the electron-lattice couplings, the horizontal CO is more stabilized and it becomes the ground state for $V_p/V_c < 0.7$. No other state is affected by these electron-lattice couplings. In Fig. 12(b), we plotted the modulations in the transfer integrals, which are consistent with the experimental values, i.e., $y_{b1} \sim 0.02$, and $y_{b2} \sim 0.01$ ²² in the region where the horizontal CO becomes the ground state. In the parameter range we have chosen, the paramagnetic metallic solution has always a higher energy than the other CO patterns at $T = 0$. In this state, the charge distribution is not uniform due to the low symmetry of the crystal structure.^{45,46} Site B is hole-rich and site C is hole-poor while the charge densities on sites A and D are the same in the metallic phase. This state is the so-called zero-gap semiconducting state where the energy band has two contact points at the Fermi energy in the Brillouin zone.^{47,48}

In above calculations, we do not show the modulations in transfer integrals such as t_{a1} and t_{b4} . In fact, we find that the distortion in t_{a1} slightly lowers the energy of the horizontal CO although the distortion is smaller than those in t_{b1} and t_{b2} . For the change in t_{b4} , the exper-

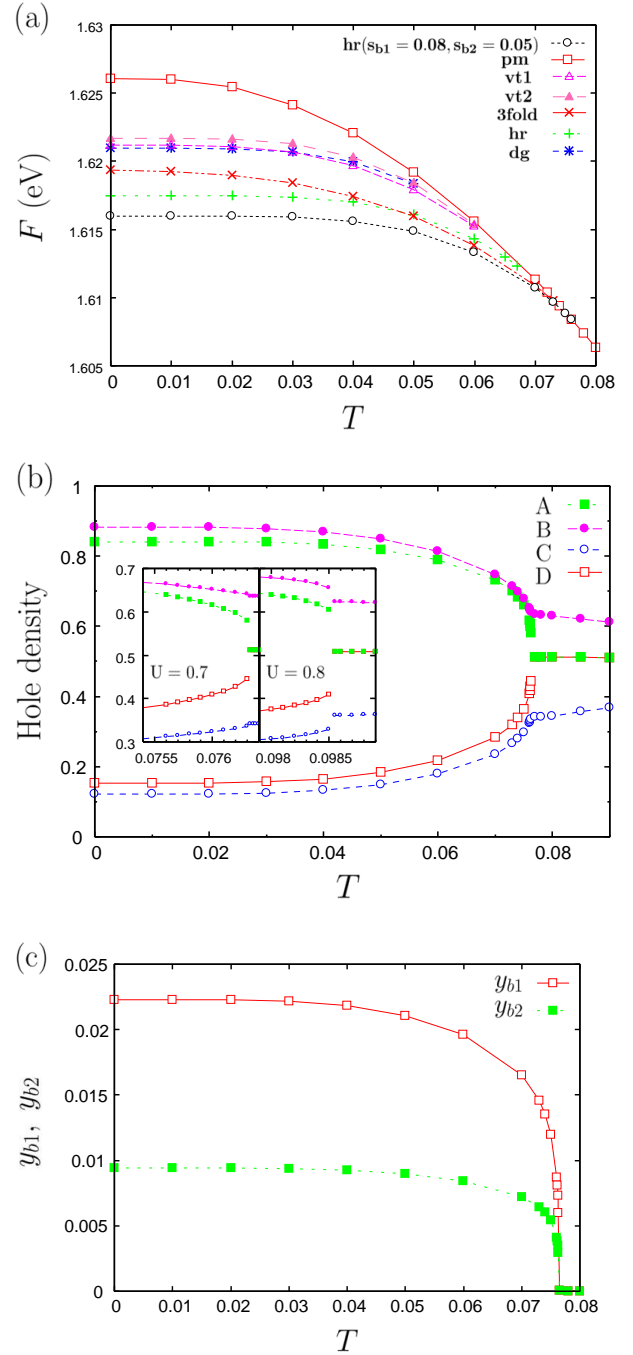


Fig. 13. (Color online) Temperature dependence of (a) free energies for various CO patterns, (b) charge density at each site, and (c) modulations y_{b1} and y_{b2} in the case of $U = 0.7$, $V_c/U = 0.4$, and $V_p/V_c = 0.6$. The inset in (b) shows the behaviors of charge densities near the transition temperature for $U = 0.7$ (left) and $U = 0.8$ (right) with fixed values of $V_c/U = 0.4$ and $V_p/V_c = 0.6$.

imentally observed modulation does not become a self-consistent solution to the Hartree-Fock calculation. This is due to the fact that the distortion gains no energy since the increasing bond $t_{B4'}$ connects the hole-poor sites C and D. Therefore, we expect that the changes in t_{b1} and t_{b2} have a major role in stabilizing the horizontal CO and the obtained results are qualitatively unchanged by other modulations.

Finally, we consider the case of finite temperatures. As discussed above, the anisotropy in V_p/V_c determines

the stability of the CO states as in the case of the θ -type salt. For $V_p/V_c \sim 1.0$ the 3-fold state is stable, while the horizontal CO is stable when V_p/V_c is small. In the latter case, a phase transition occurs from the paramagnetic metallic state to the horizontal CO. The temperature dependence of the free energies of various CO patterns for $V_p/V_c = 0.6$ is shown in Fig. 13(a). We see that the transition takes place at $T_c \sim 0.076$. The temperature dependences of the order parameters and lattice displacements are shown in Figs. 13(b) and 13(c), respectively. In the paramagnetic metallic phase, the charge densities on sites A and D are the same and the modulations are absent, while these sites are distinct from each other in the horizontal CO phase accompanied by the modulations in the transfer integrals. If Holstein-type electron-lattice couplings were present, the charge disproportionation would make a difference among the site energies at sites A, B and C, even in the metallic phase. For $T > T_c$, the contact points in the zero-gap state deviate from the Fermi energy, accompanied with thermally blurred small Fermi pockets. Below the transition temperature, the spins on the stripes are weakly antiferromagnetic, and the spin order grows towards $T = 0$. The transition is of first order although the discontinuity in the order parameters is small. In the inset of Fig. 13(b), we show the behaviors of hole-densities near T_c for $U = 0.7$ and $U = 0.8$ by fixing the ratios $V_c/U = 0.4$ and $V_p/V_c = 0.6$. The first-order transition is more evident in the case of large Coulomb interactions. Note that when we take much larger values of the electron-lattice couplings, T_c becomes higher and the transition from the paramagnetic metal to the paramagnetic horizontal CO becomes continuous. We also find that, in the present case of $U = 0.7$ the CO transition becomes continuous without electron-lattice couplings, which indicates that the lattice effect can alter the order of the transition.

A first-order transition from the charge disproportionated metallic state to the horizontal CO accompanied by the lattice distortion is consistent with the experimental findings in α -(ET)₂I₃. As for the spin degrees of freedom, the antiferromagnetic spin order is obtained in the calculated CO state whereas the spin gap is experimentally observed below T_c in the material.¹⁷ Although this result is due to the Hartree-Fock approximation which does not take account of quantum fluctuations, the spin-singlet formation below T_c can be expected by the fact that the spins on the horizontal stripes along $t_{B2'}$ and t_{B3} bonds form alternating Heisenberg chains as discussed by Seo.²⁹ Experimentally, a CO with long periodicity such as the 3-fold CO is not observed in this compound although the present calculation shows that it is stable for $V_p/V_c \sim 1.0$. As in the case of the θ -type salt, the effects of fluctuations may further stabilize the horizontal CO even in the region of $V_p/V_c \sim 1.0$.

4. Summary and Conclusions

In the present paper, we study the role of the lattice degrees of freedom to the formation of CO in the quasi-two-dimensional organic conductors θ -(ET)₂RbZn(SCN)₄ and α -(ET)₂I₃. By taking account of Peierls-type electron-lattice couplings that cause the experimentally

observed lattice modulation in each compound, we investigate the relevant extended Hubbard model within the Hartree-Fock approximation. It is found that the electron-lattice couplings stabilize the horizontal CO for both compounds, which is consistent with the experimental observations. For θ -(ET)₂RbZn(SCN)₄, the effect of the lattice distortion is crucial to realize the horizontal CO, since it does not become the ground state without electron-lattice couplings. The combined contributions of electron and lattice degrees of freedom to the CO transition are in fact suggested by the recent dielectric permittivity measurement.⁴⁹ Our results indicate that the s_ϕ distortion, which corresponds to the molecular rotation, is the most important among the three couplings in order to obtain the horizontal CO. This result is also qualitatively consistent with the exact-diagonalization study⁴¹ for eq. (1) on small clusters. At finite temperatures, a first-order metal-insulator transition is obtained, which is related to the CO transition in θ -(ET)₂RbZn(SCN)₄. For α -(ET)₂I₃, on the other hand, the horizontal CO is already stable if we consider the full band structure and the anisotropy in the nearest neighbor Coulomb interactions, although the electron-lattice couplings further lower the energy of this CO. We have shown a finite-temperature first-order transition from the paramagnetic metallic state to the horizontal CO with modulations in the transfer integrals. This result agrees with the experimental findings on α -(ET)₂I₃. Although the antiferromagnetic spin order is artificially obtained in the Hartree-Fock calculation, the spin gap behavior, which is observed in the material, is indeed expected since the exchange couplings between the neighboring spins on the horizontal stripe are alternating as pointed out previously.²⁹

The contrastive role of the lattice degrees of freedom in each compound would appear in the different natures of the CO phase transitions. θ -(ET)₂RbZn(SCN)₄ in the metallic phase has a simple band structure with higher symmetry than that of α -(ET)₂I₃, and various COs compete with each other. When the 3-fold CO fluctuations are dominant at high temperatures as suggested by the present calculation, it is natural to expect that the transition to the horizontal CO accompanies a large structural distortion because it requires the considerable replacement of the charge patterns with different unit cells. This results in the first-order transition with large discontinuity as observed experimentally. On the other hand, for α -(ET)₂I₃, the metallic state has already the charge disproportionation due to the complexity of transfer integrals. Even in this metallic phase, site B is hole-rich while site C is hole-poor, which is common to the charge distribution in the horizontal CO. Because of this, the CO can be realized by merely breaking the equivalence of charge densities in sites A and D within the high-temperature unit cell. This can lead to the first-order transition with small discontinuity relative to that in the θ -(ET)₂RbZn(SCN)₄.

Acknowledgment

The authors would like to thank H. Seo and S. Miyashita for helpful discussions. This work was sup-

ported by Grants-in-Aid for Scientific Research on Priority Area “Molecular Conductors” (No. 15073224), for Scientific Research (C) (No. 19540381), for Creative Scientific Research (No. 15GS0216), and the Next Generation Super Computing Project (Nanoscience Program) from the Ministry of Education, Culture, Sports, Science and Technology, Japan.

- 1) T. Ishiguro, K. Yamaji and G. Saito: *Organic Superconductors* (Springer-Verlag, Berlin, 1998) 2nd ed.
- 2) H. Seo, C. Hotta and H. Fukuyama: *Chem. Rev.* **104** (2004) 5005.
- 3) K. Miyagawa, A. Kawamoto and K. Kanoda: *Phys. Rev. B* **62** (2000) 7679.
- 4) R. Chiba, H. M. Yamamoto, T. Nakamura and T. Takahashi: *J. Phys. Chem. Solids* **62** (2001) 389.
- 5) Y. Takano, H. M. Yamamoto, K. Hiraki, T. Nakamura and T. Takahashi: *J. Phys. Chem. Solids* **62** (2001) 393.
- 6) Y. Takano, K. Hiraki, H. M. Yamamoto, T. Nakamura and T. Takahashi: *Synth. Met.* **120** (2001) 1081.
- 7) H. Mori, S. Tanaka and T. Mori: *Phys. Rev. B* **57** (1998) 12023.
- 8) H. Tajima, S. Kyoden, H. Mori and S. Tanaka: *Phys. Rev. B* **62** (2000) 9378.
- 9) N. L. Wang, H. Mori, S. Tanaka, J. Dong, and B. P. Clayman: *J. Phys.: Condens. Matter* **13** (2001) 5463.
- 10) K. Yamamoto, K. Yakushi, K. Miyagawa, K. Kanoda and A. Kawamoto: *Phys. Rev. B* **65** (2002) 085110.
- 11) M. Watanabe, Y. Noda, Y. Nogami and H. Mori: *J. Phys. Soc. Jpn.* **73** (2004) 116.
- 12) M. Watanabe, Y. Noda, Y. Nogami and H. Mori: *J. Phys. Soc. Jpn.* **74** (2005) 2011.
- 13) R. Chiba, K. Hiraki, T. Takahashi, H. M. Yamamoto, and T. Nakamura: *Phys. Rev. Lett.* **93** (2004) 216405.
- 14) M. Watanabe, Y. Nogami, K. Oshima, H. Mori and S. Tanaka: *J. Phys. Soc. Jpn.* **68** (1999) 2654.
- 15) Y. Nogami, J. -P. Pouget, M. Watanabe, K. Oshima, H. Mori, S. Tanaka and T. Mori: *Synth. Met.* **103** (1999) 1911.
- 16) K. Bender, K. Dietz, H. Endres, H. W. Helberg, I. Hennig, H. J. Keller, H. W. Schafer and D. Schweitzer: *Mol. Cryst. Liq. Cryst.* **107** (1984) 45.
- 17) B. Rothamel, L. Forro, J. R. Cooper, J. S. Schilling, M. Weger, P. Bele, H. Brunner, D. Schweitzer and H. J. Keller: *Phys. Rev. B* **34** (1986) 704.
- 18) H. Kino and H. Fukuyama: *J. Phys. Soc. Jpn.* **64** (1995) 1877.
- 19) H. Kino and H. Fukuyama: *J. Phys. Soc. Jpn.* **65** (1996) 2158.
- 20) R. Wojciechowski, K. Yamamoto, K. Yakushi, M. Inokuchi, and A. Kawamoto: *Phys. Rev. B* **67** (2003) 224105.
- 21) S. Moroto, K.-I. Hiraki, Y. Takano, Y. Kubo, T. Takahashi, H. M. Yamamoto, and T. Nakamura: *J. Phys. IV France* **114** (2004) 399.
- 22) T. Kakiuchi, Y. Wakabayashi, H. Sawa, T. Takahashi and T. Nakamura: *J. Phys. Soc. Jpn.* **76** (2007) 113702.
- 23) T. J. Emge, P. C. W. Leung, M. A. Beno, H. H. Wang and J. M. Williams: *Mol. Cryst. Liq. Cryst.* **138** (1986) 393.
- 24) H. Endres, J. Keller, R. Swietlik, D. Schweitzer, K. Angemund and C. Kruger: *Z. Naturforsch. A* **41** (1986) 1391.
- 25) Y. Nogami, S. Kagoshima, T. Sugano and G. Saito: *Synth. Met.* **16** (1986) 367.
- 26) Y. Nishio: unpublished.
- 27) N. A. Fortune, K. Murata, M. Ishibashi, M. Tokumoto, N. Kinoshita and H. Anzai: *Solid State Commun.* **79** (1991) 265.
- 28) S. Iwai, K. Yamamoto, A. Kashiwazaki, F. Hiramatsu, H. Nakaya, Y. Kawakami, K. Yakushi, H. Okamoto, H. Mori and Y. Nishio: *Phys. Rev. Lett.* **98** (2007) 097402.
- 29) H. Seo: *J. Phys. Soc. Jpn.* **69** (2000) 805.
- 30) R. H. McKenzie, J. Merino, J. B. Marston, and O. P. Sushkov: *Phys. Rev. B* **64** (2001) 085109.
- 31) R. T. Clay, S. Mazumdar and D. K. Campbell: *J. Phys. Soc. Jpn.* **71** (2002) 1816.
- 32) T. Mori: *J. Phys. Soc. Jpn.* **72** (2003) 1469.
- 33) J. Merino, H. Seo and M. Ogata: *Phys. Rev. B* **71** (2005) 125111.
- 34) M. Kaneko and M. Ogata: *J. Phys. Soc. Jpn.* **75** (2006) 014710.
- 35) H. Watanabe and M. Ogata: *J. Phys. Soc. Jpn.* **75** (2006) 063702.
- 36) K. Kuroki: *J. Phys. Soc. Jpn.* **75** (2006) 114716.
- 37) C. Hotta, N. Furukawa, A. Nakagawa and K. Kubo: *J. Phys. Soc. Jpn.* **75** (2006) 123704.
- 38) C. Hotta and N. Furukawa: *Phys. Rev. B* **74** (2006) 193107.
- 39) M. Udagawa and Y. Motome: *Phys. Rev. Lett.* **98** (2007) 206405.
- 40) Y. Tanaka and K. Yonemitsu: *J. Phys. Soc. Jpn.* **76** (2007) 053708.
- 41) S. Miyashita and K. Yonemitsu: *Phys. Rev. B* **75** (2007) 245112.
- 42) M. Watanabe: private communication.
- 43) T. Mori, A. Kobayashi, Y. Sasaki, H. Kobayashi, G. Saito, and H. Inokuchi: *Chem. Lett.* **13** (1984) 957.
- 44) T. Mori: *Bull. Chem. Soc. Jpn.* **73** (2000) 2243.
- 45) A. Kobayashi, S. Katayama, K. Noguchi and Y. Suzumura: *J. Phys. Soc. Jpn.* **73** (2004) 3135.
- 46) A. Kobayashi, S. Katayama, and Y. Suzumura: *J. Phys. Soc. Jpn.* **74** (2005) 2897.
- 47) S. Katayama, A. Kobayashi, and Y. Suzumura: *J. Phys. Soc. Jpn.* **75** (2006) 054705.
- 48) A. Kobayashi, S. Katayama, Y. Suzumura, and H. Fukuyama: *J. Phys. Soc. Jpn.* **76** (2007) 034711.
- 49) F. Nad, P. Monceau, and H. M. Yamamoto: *Phys. Rev. B* **76** (2007) 205101.